Spectrochimica Acta Part A: Molecular and Biomolecular Spectroscopy 125 (2014) 12–24

Contents lists available at ScienceDirect

Spectrochimica Acta Part A: Molecular and Biomolecular Spectroscopy

journal homepage: www.elsevier.com/locate/saa

Quantum mechanical and spectroscopic (FT-IR, FT-Raman, ^{1}H NMR and UV) investigations of 2-(phenoxymethyl)benzimidazole

Y. Shyma Mary [a,b,*], P.J. Jojo [b], C. Yohannan Panicker [c], Christian Van Alsenoy [d], Sanaz Ataei [e], Ilkay Yildiz [f]

[a] Department of Physics, Bharathiar University, Coimbatore, Tamil Nadu, India
[b] Department Physics, Fatima Mata National College, Kollam, Kerala, India
[c] Department of Physics, TKM College of Arts and Science, Kollam, Kerala, India
[d] Department of Chemistry, University of Antwerp, B2610 Antwerp, Belgium
[e] Ankara University, Institute of Biotechnology, 06100 Tandogan, Ankara, Turkey
[f] Ankara University, Faculty of Pharmacy, Department of Pharmaceutical Chemistry, 06100 Tandogan, Ankara, Turkey

HIGHLIGHTS

- IR, Raman spectra and NBO analysis were reported.
- The wavenumbers are calculated theoretically using Gaussian09 software.
- The wavenumbers are assigned using PED analysis.
- The geometrical parameters are in agreement with that of similar compounds.

GRAPHICAL ABSTRACT

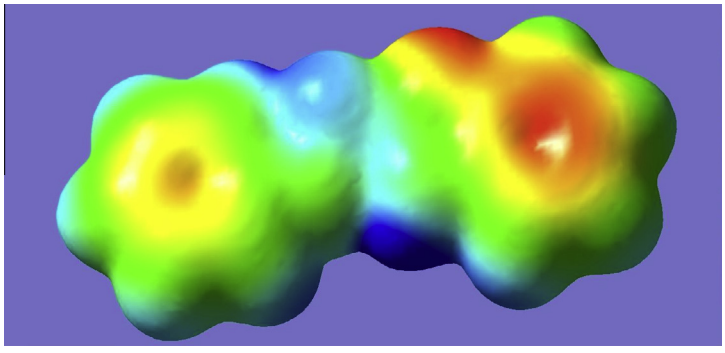

ARTICLE INFO

Article history:
Received 17 October 2013
Received in revised form 21 December 2013
Accepted 8 January 2014
Available online 24 January 2014

Keywords:
FT-IR
FT-Raman
Benzimidazole
Hyperpolarizability
PED

ABSTRACT

The optimized molecular structure, vibrational frequencies, corresponding vibrational assignments of 2-(phenoxymethyl)benzimidazole have been investigated experimentally and theoretically using Gaussian09 software package. The energy and oscillator strength calculated by time dependent density functional theory results almost compliments with experimental findings. Gauge-including atomic orbital ^{1}H NMR chemical shifts calculations were carried out and compared with experimental data. The HOMO and LUMO analysis is used to determine the charge transfer within the molecule. The stability of the molecule arising from hyper-conjugative interaction and charge delocalization has been analyzed using NBO analysis. Molecular Electrostatic Potential was performed by the DFT method and the infrared intensities and Raman activities have also been reported. Mulliken's net charges have been calculated and compared with the atomic natural charges. First hyperpolarizability is calculated in order to find its role in non-linear optics.

Introduction

Benzimidazole and its derivatives take part in several biological processes. They show pharmaceutical activity [1–7], such as lowering of blood sugar level, inhibition of phosphodiesterase-5 [8] as well as casein kinase-2 and -5 [9]. Despite a numerous attempts to develop new structural prototype in the search for more effective antimicrobials, the benzimidazoles still remain as one of the most versatile class of compounds against microbes [10–17] and, therefore, are useful substructures for further molecular exploration. The chemistry and biological profiles of various pharmacophores of 1N-substituted and 2-substituted benzimidazoles derivatives have been worked out in detail [18–29]. Benzimidazole-containing heterocyclic moieties have found

* Corresponding author at: Department of Physics, Bharathiar University, Coimbatore, Tamil Nadu, India. Tel.: +91 9995901472.
E-mail address: yshymamary@rediffmail.com (Y.S. Mary).

1386-1425/$ - see front matter © 2014 Elsevier B.V. All rights reserved.
http://dx.doi.org/10.1016/j.saa.2014.01.068

extensive use in agriculture [30]. The benzimidazole scaffold is an accepted pharmacophore and represents an important synthetic precursor in new drug discovery [31–38]. Yildiz-Oren et al. [39] synthesized 2-(phenoxymethyl)benzimidazole according to the protocol reported by King and Acheson [40] for the evaluation of microbiological activity. The minimum inhibitory concentrations (MIC) of the title compound against *Staphylococcus aureus*, *Streptococcus faecalis*, *Bacillus subtilis* as Gram-positive and *Escherichia coli*, *Klebsiella pneumoniae*, *Pseudomonas aeruginosa* as Gram negative bacteria were obtained by using twofold serial dilution technique and compared to ampicillin, amoxycillin, tetracycline, streptomycin, clotrimazole and haloprogin as standard drugs. According to this study, the title structure was found to be moderately potent either against *S. aureus*, *S. faecalis*, *B. subtilis E. coli*, *K. pneumoniae*, *P. aeruginosa* (MIC values of 25, 50, 25, 50, 25, 50 μg/mL, respectively). Besides, this compound showed more potent than the standart drug streptomycine against *S. faecalis*. Moreover, 2-(phenoxymethyl)benzimidazole exhibited significant antibacterial activity with MIC values of 25 μg/mL for the Gram-negative enterobacter *P. aeruginosa*, which is effective in nosocomial infections and often resistant to antibiotic therapy, providing higher potencies than the compared standard drugs. Considering the enormous biological importance, 2-(phenoxymethyl)benzimidazole is re-synthesized and the detailed experimental and theoretical normal Raman spectroscopy, and FTIR spectra are reported in the present work. Ab initio quantum mechanical method is at present widely used for simulating IR spectrum. Such simulations are indispensable tools to perform normal coordinate analysis so that modern vibrational spectroscopy is unimaginable without involving them and time-dependent DFT (TD-DFT) calculations have also been used for the analysis of the electronic spectrum and spectroscopic properties. The energies, degrees of hybridization, populations of the lone electron pairs of oxygen, energies of their interaction with the anti bonding π^* orbital of the benzene ring, electron density (ED) distributions and $E(2)$ energies have been calculated by NBO analysis using DFT method to give clear evidence of stabilization originating from the hyper conjugation of various intra-molecular interactions. In the present work, IR, Raman spectra, ^{1}H NMR parameters and UV–Vis spectrum of 2-(phenoxymethyl)benzimidazole are reported both experimentally and theoretically. The HOMO and LUMO analysis have been used to elucidate information regarding charge transfer within the molecule. There has been growing interest in using organic materials for nonlinear optical (NLO) devices, functioning as second harmonic generators, frequency converters, electro-optical modulators, etc. because of the large second order electric susceptibilities of organic materials. Since the second order electric susceptibility is related to first hyperpolarizability, the search for organic chromophores with large first hyperpolarizability is fully justified. The organic compounds showing high hyperpolarizability are those containing an electron donating group or an electron withdrawing group interacting through a system of conjugated double bonds. In this case, the electron withdrawing group —OPh is present in the title compound.

Experimental details

The title compound was prepared involving the reaction of *o*-phenylenediamine with phenoxyacetic acid in the presence of dehydrating agents in one step procedure as shown in Scheme 1[39,41]. During the synthesis of 2-(phenoxymethyl)benzimidazole aqueous hydrochloric acid was used as the condensation reagent according to well-known Philips' method [42]. A mixture of phenoxyacetic acid (10 mmol) and *o*-phenylenediamine (10 mmol) was boiled under reflux with stirring for 2.5 h in

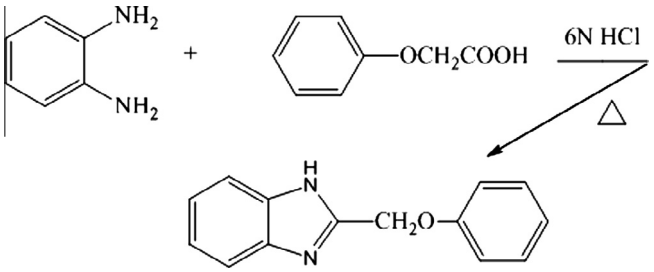

Scheme 1. Synthetic pathway of 2-(phenoxymethyl)benzimidazole.

15 ml 6 N HCl. At the end of the reaction period, the mixture was neutralized with excess of $NaHCO_3$. The collected precipitate washed with water, dried in vacuum, purified by flash chromatography, eluting with $CHCl_3$ and re-crystallized by using EtOH-H_2O. mp: 159–161 °C, yield 94%, reaction temperature 100 °C. Elemental analysis: C% 75.00 (calculated), 74.76 (found); H% 5.35 (calculated), 5.31 (found); N% 12.50 (calculated), 12.58 (found).

The FT-IR spectrum (Fig. 1) was recorded using KBr pellets on a DR/Jasco FT-IR 6300 spectrometer. The FT-Raman spectrum (Fig. 2) was obtained on a Bruker RFS 100/s, Germany. For excitation of the spectrum the emission of Nd:YAG laser was used, excitation wavelength 1064 nm, maximal power 150 mW, measurement on solid sample. ^{1}H NMR spectra were obtained with a Bruker AC 80 MHz spectrometer and TMS was used as an internal standard.

Computational details

Calculations of the title compound are carried out with Gaussian09 program [43] using the HF/6-31G*, B3LYP/6-31G* and B3LYP/SDD basis sets to predict the molecular structure and vibrational wavenumbers. Molecular geometry was fully optimized by Berny's optimization algorithm using redundant internal coordinates. Harmonic vibrational wavenumbers are calculated using the analytic second derivatives to confirm the convergence to minima on the potential surface. The wavenumber values computed at the Hartree–Fock level contain known systematic errors due to the negligence of electron correlation [44]. We therefore, have used the scaling factor value of 0.8929 for HF/6-31G* basis set. The DFT hybrid B3LYP functional and SDD methods tend to overestimate the fundamental modes; therefore scaling factor of 0.9613 has to be used for obtaining a considerably better agreement with experimental data [44]. The Stuttagart/Dresden effective core potential basis set (SDD) [45] was chosen particularly because of its advantage of doing faster calculations with relatively better accuracy and structures [46]. Then frequency calculations were employed to confirm the structure as minimum points in energy. Parameters corresponding to optimized geometry (SDD) of the title compound (Fig. 3) are given in Table S1 as Supporting material. The absence of imaginary wavenumbers on the calculated vibrational spectrum confirms that the structure deduced corresponds to minimum energy. The assignments of the calculated wavenumbers are aided by the animation option of GAUSSVIEW program, which gives a visual presentation of the vibrational modes [47]. The potential energy distribution (PED) is calculated with the help of GAR2PED software package [48]. The ^{1}H NMR data were obtained from the DFT method using basis set 6-31G*. The characterization of excited states and electronic transitions were performed using the time-dependent DFT method (TDB3LYP) on their correspondingly optimized ground state geometries. We used the time-dependent density functional theory (TD-DFT), which is found to be an accurate method for evaluating the low-lying excited states of molecules and has been thoroughly applied to solve physical and chemical problems. Vertical excitation energies were computed

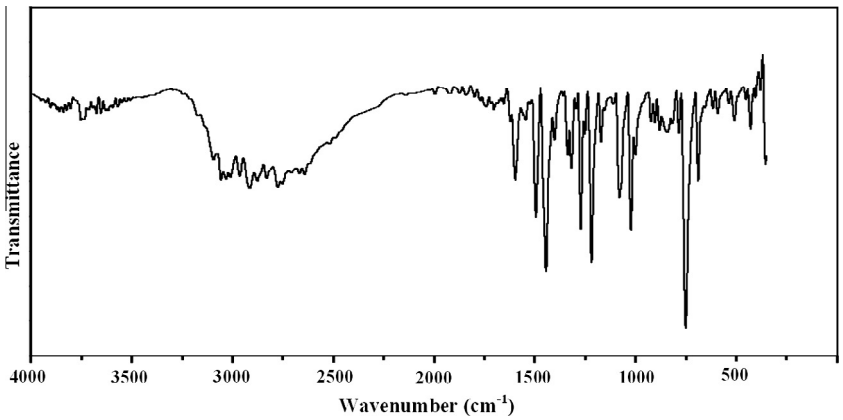

Fig. 1. FT-IR spectrum of 2-(phenoxymethyl)benzimidazole.

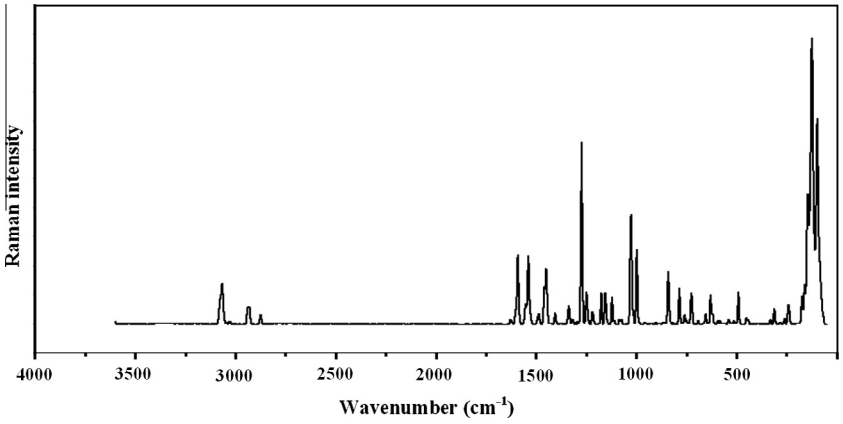

Fig. 2. FT-Raman spectrum of 2-(phenoxymethyl)benzimidazole.

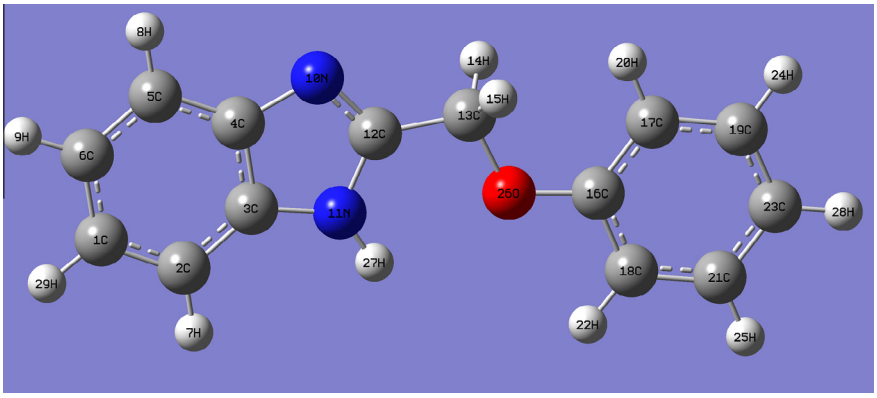

Fig. 3. Optimized geometry (SDD) of 2-(phenoxymethyl)benzimidazole.

for the first 30 singlet excited states, in order to reproduce the experimental electronic spectra. Potential energy surface scan studies have been carried out to understand the stability of planar and non-planar structures of the molecule.

Results and discussion

IR and Raman spectra

The observed IR and Raman bands, calculated (scaled) wavenumbers and assignments are given in Table 1. The C═N stretching bands [49–52] are expected in the range 1672–1566 cm^{-1}. Saxena et al. [50] reported a value 1608 cm^{-1} for polybenzodithiazole and Klots and Collier [53] reported a value of 1517 cm^{-1} for benzoxazole as υC═N stretching mode. Yang et al. [54] reported a band at 1626 cm^{-1} in the IR spectrum as υC═N for the oxazole ring. For the title compound, the SDD calculations give υC═N mode at 1522 cm^{-1}, 1523 cm^{-1} in IR and 1517 cm^{-1} in Raman which is in agreement with reported literature [55].

In aromatic compounds the υNH appears in the region 3400 ± 40 cm^{-1} [56]. For the title compound the SDD calculation give a value of 3546 cm^{-1} for this υNH mode and a band is observed in the IR spectrum at 3547 cm^{-1}. N—H group show bands

Table 1
Vibrational assignments of 2-(phenoxymethyl)benzimidazole.

HF/6-31G*			B3LYP/6-31G*			B3LYP/SDD			IR	Raman assignments	
υ	IR_I	R_A	υ	IR_I	R_A	υ	IR_I	R_A	υ	υ	–
3526	129.14	59.15	3552	84.07	88.26	3546	97.08	91.85	3547	–	υNH(99)
3040	0.16	272.64	3114	2.31	219.41	3116	3.51	316.34	3174	–	υCHII(99)
3037	16.19	6.22	3108	6.37	292.03	3108	22.69	243.46	–	–	υCHI(94)
3035	17.28	208.15	3108	27.82	16.59	3107	24.49	6.47	–	–	υCHII(93)
3025	39.15	80.22	3098	35.87	82.22	3099	33.70	41.82	–	–	υCHII(99)
3023	30.02	111.41	3096	29.94	126.69	3098	29.09	78.60	3094	–	υCHI(97)
3010	16.36	109.41	3083	14.56	117.72	3084	13.34	93.19	–	–	υCHI(97)
3010	13.01	115.75	3083	12.69	127.16	3082	10.39	104.88	–	–	υCHII(100)
3001	1.40	43.22	3075	2.05	43.66	3074	2.51	30.26	–	3075	υCHII(91)
2998	1.28	50.40	3072	0.61	50.82	3071	0.67	35.63	3056	3066	υCHI(96)
2924	17.91	51.89	29,621	19.25	59.82	2978	19.29	45.19	2968	2981	$υ_{as}CH_2$(100)
2878	9.08	136.42	2919	13.16	243.55	2925	18.58	256.50	2912	2935	$υ_sCH_2$(100)
1635	22.14	5.09	1619	9.54	5.05	1609	7.29	4.73	1620	1628	υPhI(57), υPhII(15)
1614	94.91	21.27	1598	66.05	16.89	1588	84.33	19.61	1594	1590	υPhII(67), δCHII(13)
1600	25.39	16.13	1584	31.97	30.82	1572	31.36	42.76	–	–	υPhII(54), δCHII(11)
1595	1.79	40.47	1579	0.35	50.82	1569	0.41	50.37	1543	1568	υPhI(56), υC=N(23)
1571	94.62	113.24	1531	58.12	153.10	1522	56.75	168.60	1523	1517	υC=N(54), υPhI(17)
1503	79.35	3.09	1497	34.79	7.99	1469	20.10	8.23	1493	1480	$δCH_2$(50), δCHII(23)
1491	45.03	7.56	1484	73.80	21.08	1458	401.28	10.43	–	1457	υPhII(58), δCHII(25)
1487	8.68	9.64	1481	0.55	18.39	1455	16.95	9.93	1442	1449	υPhI(50), δCHI(33)
1460	5.56	2.06	1457	3.33	2.39	1428	5.81	2.11	–	–	υPhII(53), δCHII(23)
1455	27.64	10.81	1442	17.62	29.39	1420	27.36	32.11	1400	1425	υPhI(63), δCHI(20)
1419	112.63	1.32	1395	76.41	2.89	1384	64.05	2.91	–	1370	υCN(12), $δCH_2$(54), δNH(12), δCHI(10)
1365	139.39	5.01	1364	20.01	19.17	1357	27.79	13.10	1357	–	υPhI(50), δCHI(16)
1342	0.70	1.34	1341	105.12	8.39	1338	91.89	5.61	1335	1336	δNH(47), υPhII(21)
1328	51.23	13.02	1336	2.89	3.05	1323	20.95	5.09	1315	1314	υPhII(42), δCHII(29)
1289	1.03	17.12	1314	0.56	1.81	1303	2.06	0.52	1292	1301	δCHII(48), δPhII(21)
1252	263.89	21.66	1303	10.37	2.69	1286	16.97	3.03	1270	1272	υCN(46), υPhI(43)
1238	81.85	62.34	1251	30.51	85.16	1241	28.94	102.74	1249	1242	υCN(38), δCHI(41)
1226	5.76	11.81	1219	357.18	4.34	1205	314.07	3.06	1216	1219	$δCH_2$(46), δCHII(26)
1224	31.66	21.38	1212	14.35	38.36	1202	72.86	26.77	1199	1199	δNH(18), υCN(52)
1222	102.54	2.55	1191	2.91	13.80	1187	1.39	11.43	–	–	υCOC(55), δNH(18)
1194	21.87	9.91	1189	58.19	7.89	1181	35.87	10.66	–	1176	δNH(23), υCN(28), δPhI(18)
1178	4.34	5.63	1182	13.99	5.05	1167	23.99	5.26	1169	–	δCHII(75)
1147	3.83	1.33	1172	12.10	3.94	1155	10.03	2.75	1152	1154	δCHII(80), υPhII(12)
1146	8.28	9.08	1159	2.61	17.43	1145	1.99	13.78	–	1120	δCHI(77), υPhI(16)
1111	0.27	11.11	1112	0.77	13.10	1095	2.65	11.17	1107	1109	δCHI(52), υPhI(32)
1077	13.19	0.71	1083	8.99	1.61	1068	14.95	1.07	1077	1084	υPhI(38), δCHII(30), δCHI(32)
1048	1.51	0.59	1023	19.44	10.61	1012	0.09	0.38	1020	1026	δCHII(57), δCHI(18)
1038	0.11	0.85	1022	0.07	0.87	1007	38.71	13.13	1007	–	υPhII(51), δCHII(22)
1038	75.16	5.08	1011	113.87	19.05	996	14.19	30.85	998	997	δPhII(27), δPhI(42)

(*continued on next page*)

Table 1 (*continued*)

HF/6-31G*			B3LYP/6-31G*			B3LYP/SDD			IR	Raman assignments	
υ	IR_I	R_A	υ	IR_I	R_A	υ	IR_I	R_A	υ	υ	–
1037	0.02	0.98	1003	21.03	35.96	991	0.76	0.27	–	–	γCHII(81), τPhII(15)
1019	0.01	0.25	989	6.29	21.68	988	13.69	23.26	–	–	υCOC(51), δPhII(22)
1017	1.58	4.24	982	0.39	0.34	982	0.02	0.25	–	–	γCHI(87), τPhI(11)
1007	4.53	54.98	974	32.57	0.65	972	0.68	37.75	–	–	δPhII(42), υPhII(14)
994	6.01	0.09	972	0.01	0.09	968	0.05	0.08	–	–	γCHII(90)
989	2.06	16.97	953	0.01	0.41	960	20.78	1.51	959	958	υCOC(18), δCH_2(52)
981	8.76	4.03	929	2.81	0.44	944	4.90	1.07	921	–	γCHI(91)
943	18.25	1.82	889	8.48	2.74	898	9.57	0.15	902	902	γCHII(77), τPhII(13)
899	0.28	1.76	885	2.58	1.85	870	1.83	1.59	878	879	δPhI(61), δRingII(11)
888	1.64	1.86	853	0.01	3.58	862	0.04	0.98	841	864	γCHI(74), τPhI(11)
864	0.05	2.83	820	0.02	4.55	825	0.20	0.01	814	830	γCHII(99)
821	29.63	3.86	819	9.92	1.25	808	7.07	4.56	–	811	υPhI(30), δRingII(34)
808	6.11	35.59	809	13.59	41.92	795	17.51	42.97	783	785	υPhII(16), δPhII(28), δCCO(19)
789	1.39	2.66	757	8.86	2.48	771	9.05	0.98	–	–	τPhI(52), τRingII(31)
785	199.51	0.07	754	105.51	0.30	758	147.55	0.07	769	759	γCHII(57), τPhII(21), γCO(16)
782	68.58	0.94	750	58.48	2.63	757	78.73	0.28	749	749	γCHI(78)
707	33.54	1.26	709	2.69	5.04	697	3.67	5.74	–	690	δRingII(33), δPhI(32)
706	2.99	5.87	689	19.79	0.94	687	37.14	0.17	687	–	τPhII(69), γCHII(20)
685	50.51	4.72	648	19.42	2.62	668	84.64	0.31	–	670	γNH(95)
656	80.80	1.19	647	97.18	1.55	650	0.01	2.55	652	654	τRingII(52), γCC(23)
624	0.26	3.14	622	0.37	3.20	609	0.42	10.93	613	619	δRingII(42), δPhI(35)
622	0.72	10.82	619	0.31	10.49	608	0.62	7.99	–	–	δPhII(85)
598	0.53	2.06	597	0.82	2.47	584	0.50	4.52	589	581	δPhII(41), δPhI(28)
589	4.18	0.04	578	0.61	0.07	577	0.92	0.08	–	545	τPhI(65), τRingII(18)
515	5.51	0.64	508	2.09	3.54	501	12.56	5.32	507	–	δCC(21), δPhI(21), δCOC(29)
505	16.74	4.18	505	15.34	1.87	499	10.59	0.24	–	491	γCO(41), τPhII(40)
504	0.63	1.64	501	4.85	0.42	498	4.29	0.77	487	491	δPhII(39), δPhI(33)
447	6.34	0.53	432	4.08	0.52	433	8.28	0.56	426	442	τPhI(58), τRingII(28)
424	0.03	0.16	415	0.03	0.14	410	0.06	0.07	413	–	τPhII(84)
403	5.05	2.38	405	4.89	2.69	401	5.37	3.42	405	398	δCO(43), δPhI(28)
317	0.15	0.55	306	0.13	0.26	311	0.11	0.08	–	314	γCC(31), τPhI(27), τRingII(16)
259	5.29	0.67	252	3.49	0.80	249	4.33	0.64	–	255	τPhI(69), τRingII(22)
240	1.09	2.90	238	0.69	2.95	236	0.86	3.53	–	238	δCC(38), δPhI(28)
236	0.95	2.99	232	0.75	2.56	229	0.17	1.97	–	–	τPhII(57), τCC(15)
166	2.24	0.79	170	2.11	0.72	168	2.16	0.90	–	173	δCO(53), δCC(15)
145	10.67	4.42	142	8.35	4.32	149	11.27	2.66	–	144	τRingII(34), τCC(29), γCC(16)
69	3.99	8.91	74	1.86	9.99	80	1.76	9.20	–	96	τCO(69), τCC(10)
56	0.92	0.26	58	1.03	0.41	58	1.11	0.42	–	65	δCC(51), δCO(26)
29	0.58	0.78	28	0.09	0.51	31	0.04	0.28	–	–	τCC(82)

Table 1 (*continued*)

HF/6-31G*			B3LYP/6-31G*			B3LYP/SDD			IR	Raman assignments	
υ	IR_I	R_A	υ	IR_I	R_A	υ	IR_I	R_A	υ	υ	–
15	3.04	1.26	10	4.09	2.02	18	3.99	1.36	–	–	τCC(61), γNH(15), γCC(14)

υ – stretching; δ – in-plane deformation; γ – out-of-plane deformation; τ – torsion; as – asymmetric; s – symmetric; PhI – di-substituted benzene ring; PhII – mono substituted benzene ring; RingIII – benzimidazole ring; potential energy distribution (%) is given in brackets in the assignment column; IR_I – IR intensity; R_A – Raman activity.

at 1510–1500, 1350–1250 and 740–730 cm^{-1} [57]. According to literature, if N—H is a part of a closed ring [57,58] the C—N—H deformation band is absent in the region 1510–1500 cm^{-1}. For the title compound the C—N—H deformation band is observed at 1336 cm^{-1} in the Raman spectrum, 1335 cm^{-1} in the IR spectrum and at 1338 cm^{-1} theoretically (SDD). The out of plane NH deformation is expected in the region 650 ± 50 cm^{-1} [56] and the band at 670 cm^{-1} in the Raman spectrum and at 668 cm^{-1} theoretically (SDD) are assigned as this mode. Minitha et al. [59] reported υNH at 3469 cm^{-1}, δNH at 1300 cm^{-1} and γNH at 535 cm^{-1}. Panicker et al. reported the out-of-plane bending mode of NH at 746 cm^{-1}, theoretically [60]. Kim et al. reported [61] NH deformation bands at 549, 1484 cm^{-1} in the Raman spectrum and at 556, 1495 cm^{-1} theoretically for benzimidazole and Malek et al. [62] reported modes at 1394, 680 cm^{-1} theoretically as NH deformation.

Primary aromatic amines with nitrogen directly on the ring absorb strongly at 1330–1260 cm^{-1} due to stretching of the phenyl carbon–nitrogen bond [63]. Sandhyarani et al. [64] reported υCN at 1318 cm^{-1} for 2-mercaptobenzothiazole. For the title compound υCN are assigned at 1270, 1249, 1199 cm^{-1} in the IR spectrum, 1272, 1242, 1199 cm^{-1} in the Raman spectrum and the calculated (SDD) values are 1286, 1241, 1202 cm^{-1}. These modes are not pure but contain a significant contribution from other modes. For 5-nitro-2-(4-nitrobenzyl) benzoxazole, C—N stretching vibrations are observed in the region at 1228–1195 cm^{-1} [55]. CN stretching modes are reported at 1268, 1220, 1151 cm^{-1} theoretically for benzimidazolium salts by Malek et al. [62].

For the title compound, as expected the asymmetric C—O—C stretching vibration is assigned at 1187 cm^{-1} and the symmetric stretching mode at 988 cm^{-1} (SDD) theoretically [51]. The C—O—C stretching modes are reported at 1250 and 1073 cm^{-1} for 2-mercpatobenzoxazole [65]. Bhagyasree et al. [55] reported C—O—C stretching modes at 1144, 1063 (IR), 1146, 1066 (Raman) and at 1153, 1079 cm^{-1} theoretically (SDD).

The vibrations of the CH_2 group, the asymmetric stretch $\upsilon_{as}CH_2$, symmetric stretch υ_sCH_2, scissoring vibration δCH_2, appear in the region 2945 ± 45, 2885 ± 45 and 1445 ± 35 cm^{-1}, respectively [56,63]. The SDD calculations give $\upsilon_{as}CH_2$ at 2978 cm^{-1} and υ_sCH_2 at 2925 cm^{-1}. The bands observed at 2968, 2912 cm^{-1} (IR) and 2981, 2935 cm^{-1} (Raman) are assigned as asymmetric and symmetric CH_2 modes, respectively. In the present case, the band observed at 1493 cm^{-1} in the IR, 1480 in Raman spectrum and 1469 cm^{-1} (SDD) are assigned as the scissoring mode of CH_2. Bands of hydrocarbons due to CH_2 twisting and wagging vibrations are observed in the region 1180–1390 cm^{-1} [51,63]. The CH_2 wagging and twisting modes are assigned at 1384 and 1205 cm^{-1} (SDD), 1216 cm^{-1} (IR), 1370, 1219 cm^{-1} (Raman) respectively. The band calculated at 960 cm^{-1} is assigned as the rocking mode of CH_2.

The existence of one or more aromatic rings in a structure is normally readily determined from the C—H and C=C—C ring related vibrations. The C—H stretching occurs above 3000 cm^{-1} and is typically exhibited as a multiplicity of weak to moderate bands, compared with the aliphatic C—H stretch [66]. In the present case, the SDD calculations give υC—H modes in the range of 3071–3116 cm^{-1}. The bands observed at 3056, 3094, 3174 cm^{-1} in the IR spectrum and at 3066, 3075 cm^{-1} in the Raman spectrum are assigned as the υC—H modes of the benzene rings.

Since the identification of all the normal modes of vibration of large molecules is not trivial, we tried to simplify the problem by considering each molecule as substituted benzene. Such an idea has already been successfully utilized by several workers for the vibrational assignments of molecules containing multiple homo and hetero aromatic rings [67–71]. In the following discussion, the mono-substituted and di-substituted phenyl rings are designated as rings PhII and PhI, respectively and benzimidazole as ring-III. The modes in the two phenyl rings will differ in wavenumber and the magnitude of splitting will depend on the strength of interactions between different parts (internal coordinates) of the two rings. For some modes, this splitting is so small that they may be considered as quasi-degenerate and for the other modes a significant amount of splitting is observed. Such observations have already been reported [67–69,72].

The benzene ring possesses six ring stretching vibrations, of which the four with the highest wavenumbers (occurring respectively near 1600, 1580, 1490 and 1440 cm^{-1}) are good group vibrations. In the absence of ring conjugation, the band near 1580 cm^{-1} is usually weaker than that at 1600 cm^{-1}. The fifth ring stretching vibration is active near 1355 ± 35 cm^{-1}, a region which overlaps strongly with that of the CH in-plane deformation and the intensity is in general, low or medium [56,73]. The sixth ring stretching vibration or ring breathing mode appears as a weak band near 1000 cm^{-1} in mono-substituted benzenes [56].

For the title compound, the bands observed at 1594, 1315 cm^{-1} in the IR and 1590, 1457, 1314 cm^{-1} in the Raman spectrum are assigned as υPhII modes with 1588, 1572, 1458, 1428, 1323 cm^{-1} as SDD values. For the title compound, PED analysis gives the ring breathing mode of PhII at 1007 cm^{-1} [74]. For the phenyl ring PhI, the bands observed at 1620, 1543, 1442, 1400, 1270 cm^{-1} in the IR spectrum and at 1628, 1568, 1449, 1425, 1272 cm^{-1} in the Raman spectrum were assigned as υPhI. Also SDD calculations give these modes at 1609, 1569, 1455, 1420, 1286 cm^{-1}, which are in agreement with literature [56]. In ortho substitution the ring breathing mode has three frequency intervals according to whether both substituents are heavy, or one of them is heavy while the other is light, or both of them are light. In the first case the interval is 1100–1130, in the second case 1020–1070 cm^{-1}, while in the third case it is between 630 and 780 cm^{-1} [73]. The bands observed at 1077 cm^{-1} in the IR spectrum, 1084 cm^{-1} in the Raman spectrum and at 1068 cm^{-1} (SDD) is assigned as the ring breathing mode for PhI ring in the present case.

The CH in-plane bending for the phenyl rings are expected above 1000 cm^{-1} [56] and bands observed at 1077, 1107, 1249 (IR), 1084, 1109, 1120, 1242 (Raman) and 1020, 1077, 1152, 1169, 1292 (IR), 1026, 1084, 1154, 1301 cm^{-1} (Raman) are assigned as in-plane CH modes for the rings PhI and PhII, respectively. The corresponding calculated values (SDD) are 1068, 1095, 1145, 1241 for PhI and 1012, 1068, 1155, 1167, 1303 cm^{-1} for PhII rings. The CH out-of-plane deformations [74] are observed between 1000 and 700 cm^{-1}. Generally, the C—H out-of-plane deformations with the highest wavenumbers have a weaker intensity

Table 2
Second-order perturbation theory analysis of Fock matrix in NBO basis corresponding to the intra molecular bonds of the title compound.

Donor (*i*)	Type	ED/e	Acceptor (*j*)	Type	ED/e	$E(2)$[a]	$E(j)-E(i)$[b]	$F(i,j)$[c]
C1—C2	σ	1.98	C1—C6	σ*	0.02	2.50	1.25	0.05
–	–	–	C2—C3	–	0.02	3.39	1.26	0.06
–	–	–	C3—N11	–	0.03	6.89	1.11	0.08
C1—C2	π	1.73	C3—C4	π*	0.48	20.10	0.27	0.07
–	–	–	C5—C6	–	0.31	17.50	0.29	0.06
C1—C6	σ	1.98	C1—C2	σ*	0.01	2.63	1.25	0.05
–	–	–	C2—H7	–	0.01	2.40	1.14	0.05
–	–	–	C5—C6	–	0.01	2.62	1.26	0.05
–	–	–	C5—H8	–	0.01	2.35	1.16	0.05
C1—H29	σ	1.98	C2—C3	σ*	0.02	3.69	1.09	0.06
–	–	–	C5—C6	–	0.01	3.52	1.10	0.06
C2—C3	σ	1.98	C1—C2	σ*	0.01	2.61	1.29	0.05
–	–	–	C1—H29	–	0.01	2.12	1.19	0.05
–	–	–	C3—C4	–	0.04	4.68	1.24	0.07
–	–	–	C3—N11	–	0.03	2.48	1.13	0.05
C2—H7	σ	1.98	C1—C6	σ*	0.02	3.44	1.09	0.06
–	–	–	C3—C4	–	0.04	4.06	1.06	0.06
C3—C4	σ	1.97	C2—C3	σ*	0.02	4.63	1.25	0.07
–	–	–	C2—H7	–	0.01	2.45	1.14	0.05
–	–	–	C4—C5	–	0.02	3.84	1.26	0.06
–	–	–	C5—H8	–	0.01	2.24	1.15	0.05
–	–	–	N11—H27	–	0.02	4.14	1.13	0.06
C3—C4	π	1.60	C1—C2	π*	0.33	18.87	0.28	0.07
–	–	–	C5—C6	–	0.31	18.87	0.29	0.07
–	–	–	N10—C12	–	0.35	14.21	0.25	0.05
C3—N11	σ	1.98	C2—C3	σ*	0.02	2.35	1.37	0.05
–	–	–	C4—C5	–	0.02	2.48	1.39	0.05
–	–	–	C12—C13	–	0.03	3.91	1.21	0.06
C4—C5	σ	1.98	C3—C4	σ*	0.04	3.71	1.22	0.06
–	–	–	C4—N10	–	0.02	2.35	1.13	0.05
–	–	–	C5—C6	–	0.01	2.59	1.28	0.05
–	–	–	C6—H9	–	0.01	2.25	1.17	0.05
C4—N10	σ	1.98	C2—C3	σ*	0.02	2.48	1.32	0.05
–	–	–	C4—C5	–	0.02	2.30	1.34	0.05
–	–	–	C12—C13	–	0.03	1.09	1.16	0.08
C5—C6	σ	1.98	C1—C6	σ*	0.02	2.53	1.24	0.05
–	–	–	C4—C5	–	0.02	3.01	1.27	0.06
–	–	–	C4—N10	–	0.02	5.44	1.12	0.07
C5—C6	π	1.71	C1—C2	π*	0.33	20.44	0.27	0.07
–	–	–	C3—C4	–	0.48	18.88	0.26	0.07
C5—H8	σ	1.98	C1—C6	σ*	0.02	3.62	1.07	0.06
–	–	–	C3—C4	–	0.04	4.18	1.04	0.06
C6—H9	σ	1.98	C1—C2	σ*	0.01	3.63	1.09	0.06
–	–	–	C4—C5	–	0.02	3.60	1.10	0.06
N10—C12	σ	1.98	C4—C5	σ*	0.02	4.81	1.43	0.07
–	–	–	N11—H27	–	0.02	2.16	1.30	0.05
N10—C12	σ	1.88	C3—C4	σ*	0.48	17.07	0.33	0.07
N11—C12	π	1.99	C2—C3	π*	0.02	4.76	1.39	0.07
N11—H27	σ	1.99	N10—C12	σ*	0.01	2.33	1.23	0.05
C12—C13	σ	1.98	C4—N10	σ*	0.02	2.48	1.12	0.05
–	–	–	C16—O26	–	0.03	2.19	0.97	0.04
C13—H14	σ	1.98	N10—C12	σ*	0.35	3.67	0.54	0.04
–	–	–	N11—C12	–	0.05	2.19	0.96	0.04
C13—H15	π	1.98	N10—C12	π*	0.35	3.66	0.54	0.04
–	–	–	N11—C12	–	0.05	2.19	0.96	0.04
C13—O26	σ	1.99	N10—C12	σ*	0.01	2.91	1.34	0.06
–	–	–	C16—C18	–	0.02	2.27	1.36	0.05
C16—C17	π	1.98	C16—C18	π*	0.02	4.44	1.28	0.07
–	–	–	C17—C19	–	0.02	2.81	1.29	0.06
–	–	–	C17—H20	–	0.01	1.56	1.18	0.04
–	–	–	C18—H22	–	0.01	1.86	1.18	0.04
C16—C17	σ	1.68	C18—C21	σ*	0.32	17.44	0.29	0.06
–	–	–	C19—C23	–	0.33	20.96	0.29	0.07
C16—C18	σ	1.97	C13—O26	σ*	0.01	2.69	0.93	0.05
–	–	–	C16—C17	–	0.03	4.24	1.26	0.07
–	–	–	C17—H20	–	0.01	2.22	1.17	0.05
–	–	–	C18—C21	–	0.01	2.55	1.28	0.05
–	–	–	C21—H25	–	0.01	2.15	1.18	0.05
C17—C19	σ	1.97	C16—C17	σ*	0.03	3.24	1.25	0.06
–	–	–	C16—O26	–	0.03	5.04	0.99	0.06
–	–	–	C19—C23	–	0.02	2.68	1.27	0.05
–	–	–	C23—H28	–	0.01	2.21	1.17	0.05
C17—H20	σ	1.98	C16—C18	σ*	0.02	3.80	1.09	0.06
–	–	–	C19—C23	–	0.02	3.33	1.11	0.05

Table 2 (*continued*)

Donor (*i*)	Type	ED/e	Acceptor (*j*)	Type	ED/e	*E*(2)[a]	*E*(*j*) − *E*(*i*)[b]	*F*(*i*,*j*)[c]
C18—C21	σ	1.98	C16—C18	σ*	0.02	2.75	1.26	0.05
–	–	–	C16—O26	–	0.03	3.95	0.99	0.06
–	–	–	C21—C23	–	0.02	2.66	1.26	0.05
–	–	–	C23—H28	–	0.01	2.19	1.17	0.05
C18—C19	π	1.70	C16—C17	π*	0.39	22.37	0.26	0.07
–	–	–	C19—C23	–	0.33	17.98	0.28	0.06
C18—H22	σ	1.98	C16—C17	σ*	0.03	4.10	1.08	0.06
–	–	–	C21—C23	–	0.02	4.43	1.09	0.06
C19—C23	σ	1.98	C17—C19	σ*	0.02	2.71	1.26	0.05
–	–	–	C17—H20	–	0.01	2.24	1.16	0.05
–	–	–	C21—C23	–	0.02	2.61	1.26	0.05
–	–	–	C21—H25	–	0.01	2.28	1.16	0.05
C19—C23	π	1.68	C16—C17	π*	0.39	18.45	0.26	0.06
–	–	–	C18—C21	–	0.32	21.88	0.27	0.07
C19—H24	σ	1.98	C16—C17	σ*	0.03	3.80	1.08	0.06
C21—C23	σ	1.98	C18—C21	σ*	0.01	2.70	1.27	0.05
–	–	–	C18—H22	–	0.01	2.41	1.16	0.05
–	–	–	C19—C23	–	0.02	2.62	1.26	0.05
–	–	–	C19—H24	–	0.01	2.36	1.16	0.05
C21—H25	σ	1.98	C16—C18	σ*	0.02	3.77	1.08	0.06
–	–	–	C19—C23	–	0.02	3.41	1.10	0.06
C23—H28	σ	1.98	C17—C19	σ*	0.02	3.66	1.09	0.06
–	–	–	C18—C21	–	0.01	3.46	1.10	0.06
LP(1)N10	n	1.93	C3—C4	σ*	0.04	5.82	0.87	0.06
–	–	–	N11—C12	–	0.05	10.11	0.76	0.08
LP(1)N11	n	1.61	C3—C4	π*	0.48	33.25	0.29	0.09
–	–	–	N10—C12	–	0.35	50.13	0.27	0.11
LP(1)O26	n	1.96	C16—C17	σ*	0.03	2.76	1.45	0.06
LP(2)O26	n	1.87	C13—H14	σ*	0.02	4.55	0.74	0.05
–	–	–	C13—H15	–	0.02	4.55	0.74	0.05
–	–	–	C16—C17	π*	0.39	26.25	0.33	0.09

[a] *E*(2) means energy of hyperconjugative interactions (stabilization energy).
[b] Energy difference between donor and acceptor *i* and *j* NBO orbitals.
[c] *F*(*i*,*j*) is the Fock matrix element between *i* and *j* NBO orbitals.

than those at lower wavenumbers. The out-of-plane CH deformation at 769 cm^{-1} and the out-of-plane ring deformation at 687 cm^{-1} in the IR spectrum form a pair of strong bands characteristics of mono-substituted benzene derivative [56,75]. In the present case bands at 902, 814, 769 cm^{-1} in the IR, at 902, 830, 759 cm^{-1} in Raman and at 991, 968, 898, 825, 758 cm^{-1} by SDD are assigned as CH out-of-plane deformations for PhII ring. In the case of 1,2-disubstituted benzenes, a strong absorption in the region 755 ± 35 cm^{-1} is observed and is due to γCH, which is assigned at 749 cm^{-1} in the IR spectrum [66]. For the title compound modes obtained at 982, 944, 862, 757 cm^{-1} by theory (SDD) with 921, 841, 749 cm^{-1} in IR and 864, 749 cm^{-1} in Raman spectra are assigned as the CH out-of-plane deformations for PhI ring. The substituent sensitive modes of the rings are also identified and assigned (Table 1).

Optimized geometry

A detailed potential energy surface (PES) scan on dihedral angles N_{10}—C_{12}—C_{13}—O_{26}, C_{12}—C_{13}—O_{26}—C_{16} have been performed at B3LYP/6-31G(d) level to reveal all possible conformations of 2-(phenoxymethyl)benzimidazole. The PES scan was carried out by minimizing the potential energy in all geometrical parameters by changing the torsion angle at every 10° for 180° rotation around the bond. The results obtained in PES scan study by varying the torsion perturbation around the CH_2 bonds are plotted in Figs. S1 and S2 (Supporting information). For the N_{10}—C_{12}—C_{13}—O_{26} rotation, the minimum energy was obtained at −180.0° in the potential energy curve of energy −725.44703 Hartrees. For the C_{12}—C_{13}—O_{26}—C_{16} rotation, the minimum energy occurs at 180.0° in the potential energy curve of energy −725.4470.

To the best of our knowledge, no X-ray crystallographic data of this molecule has yet been established. The optimized molecular structure of 2-(phenoxymethyl)benzoimidazole was determined by using Gaussian09 program. The optimized geometry is summarized in Table S1. From Table S1, it is clearly seen that the dihedral angles C_6—C_5—C_4—N_{10} and C_4—N_{10}—C_{12}—C_{13}, C_1—C_2—C_3—N_{11}, C_2—C_3—N_{11}—C_{12} are 180°. This indicates that the benzene ring I and the benzimidazole ring moieties of the title compound are planar as in the case of 2-amino-6-methylbenzothiazole [76]. For 2-amino-6-methylbenzothiazole [76] the bond lengths C_4—C_5, C_4—C_3, C_3—C_2, C_4—N_{10}, are respectively, 1.4145, 1.4333, 1.4066, 1.4110 Å. The corresponding values for the title compound are 1.4076, 1.4311, 1.405, 1.4127 Å. The SDD calculations give the bond angles C_3—C_4—N_{10}, C_4—N_{10}—C_{12}, C_3—N_{11}—C_{12}, N_{10}—C_{12}—N_{11} as 109.9, 105.0, 107.3 and 113.1° for the title compound. These values are in agreement with the bond angles reported for 2-amino-6-methylbenzothiazole [76] and for 2-amino-4-ethylbenzothiazole [77]. For 2- amino-4-methylbenzothiazole [77] the bond lengths C_3—C_4, C_{12}—N_{10}, C_4—N_{10} are 1.3916, 1.2962, 1.4173 Å, respectively.

Purkayastha and Chattopadhyay [78] reported N_{10}—C_{12}, N_{10}—C_4 bond lengths as 1.3270, 1.400 Å for benzothiazole and 1.3503, 1.407 Å for benzimidazole compounds. For the title compound we have obtained these values are 1.3305 and 1.4127 Å. The carbon–carbon bond lengths in the phenyl ring PhI lie between 1.4041 and 1.4311 Å while for phenyl ring PhII, the range is 1.4033–1.4113 Å. The CH bond length lies between 1.0859 and 1.0874 Å for PhI and 1.0852–1.0873 Å for PhII. These changes in bond lengths for the title compound can be attributed to the conjugation of the phenyl ring. Here for the title compound, benzene is a regular hexagon with bond lengths somewhere in between the normal values for a single (1.54 Å) and a double (1.33 Å) bond [79].

For the title compound, the bonds C_{12}—N_{10} = 1.3305 show typical double bond characteristics. However, C_4—N_{10} = 1.4127 Å, C_3—N_{11} = 1.3992 Å, C_{12}—N_{11} = 1.3881 Å bond length are shorter than the normal C—N single bond length of about 1.48 Å. The

shortening of the C—N bonds reveal the effects of resonance in this part of the molecule [80] and this situation can be attributed to the difference in hybridization of the different carbon atoms.

Lifshitz et al. [81] reported the bond lengths for N_{10}—C_{12}, C_3—C_2, C_4—C_5, C_3—C_4, and N_{10}—C_4 as 1.291, 1.374, 1.39, 1.4, 1.403 and 1.401 Å. The corresponding values in the present case are 1.3305, 1.405, 1.4076, 1.4311, 1.4127 Å. Corresponding values are reported as 1.2753, 1.3492, 1.359, 1.3768, 1.3879, 1.3784, 1.3892 Å [82] and 1.2727, 1.347, 1.3594, 1.3884, 1.3777, 1.3776, 1.3903 Å [49]. The bond lengths C_4—N_{10}, N_{10}—C_{12} and C_3—C_4 are found to be 1.3436, 1.3804 and 1.3827 Å for mercaptobenzoxazole [65]. For the title compound these values are respectively 1.4127, 1.3305, 1.4311 Å.

First hyperplarizability

Nonlinear optics deals with the interaction of applied electromagnetic fields in various materials to generate new electromagnetic fields, altered in wavenumber, phase, or other physical properties [83]. Organic molecules able to manipulate photonic signals efficiently are of importance in technologies such as optical communication, optical computing, and dynamic image processing [84,85]. In this context, the dynamic first hyperpolarizability of the title compound is also calculated in the present study. First hyperpolarizability is a third rank tensor that can be described by a $3 \times 3 \times 3$ matrix. The 27 components of the 3D matrix can be reduced to 10 components due to the Kleinman symmetry [86]. The components of beta are defined as the coefficients in the Taylor series expansion of the energy in the external electric field. When the electric field is weak and homogeneous, this expansion becomes

$$E = E_0 - \sum_i \mu_i F^i - \frac{1}{2}\sum_{ij} \alpha_{ij} F^i F^j - \frac{1}{6}\sum_{ijk} \beta_{ijk} F^i F^j F^k - \frac{1}{24}\sum_{ijkl} \gamma_{ijkl} F^i F^j F^k F^l + \cdots$$

where E_0 is the energy of the unperturbed molecule, F^i is the field at the origin, μ_i, α_{ij}, β_{ijk} and γ_{ijkl} are the components of dipole moment, polarizability, the first hyper polarizabilities, and second hyperpolarizibilities, respectively. The calculated first hyperpolarizability of the title compound is 2.34×10^{-30} esu, which comparable with the reported values of similar derivatives [87] and which is 18.00 times that of the standard NLO material urea (0.13×10^{-30} esu) [88]. We conclude that the title compound is an attractive object for future studies of nonlinear optical properties.

NBO analysis

The natural bond orbital (NBO) calculations were performed using NBO 3.1 program [89] as implemented in the Gaussian09 package at the DFT/B3LYP level in order to understand various second-order interactions between the filled orbital of one subsystem and vacant orbital of another subsystem, which is a measure of the inter molecular delocalization or hyper conjugation. NBO analysis provides the most accurate possible 'natural Lewis structure' picture of '*j*' because all orbital details are mathematically chosen to include the highest possible percentage of the electron density. A useful aspect of the NBO method is that it gives information about interactions of both filled and virtual orbital spaces that could enhance the analysis of intra and inter molecular interactions.

The second-order Fock-matrix was carried out to evaluate the donor–acceptor interactions in the NBO basis. The interactions result in a loss of occupancy from the localized NBO of the idealized Lewis structure into an empty non-Lewis orbital. For each donor (i) and acceptor (j) the stabilization energy ($E2$) associated with the delocalization $i \rightarrow j$ is determined as

$$E(2) = \Delta E_{ij} = q_i \frac{(F_{i,j})^2}{(E_j - E_i)}$$

$q_i \rightarrow$ donor orbital occupancy;
E_i, $E_j \rightarrow$ diagonal elements;
$F_{ij} \rightarrow$ the off diagonal NBO Fock matrix element.

In NBO analysis large $E(2)$ value shows the intensive interaction between electron-donors and electron-acceptors and greater the extent of conjugation of the whole system, the possible intensive interactions are given in Table 2. The second-order perturbation theory analysis of Fock matrix in NBO basis shows strong intra molecular hyper conjugative interactions of π electrons. The intra molecular hyper conjugative interactions are formed by the orbital overlap between n(O) and π*(C—C) bond orbital which results in ICT causing stabilization of the system. The strong intra molecular hyper conjugative interaction of C_{16}—C_{17} from of $n_2(O_{26}) \rightarrow \pi^*(C_{16}$—$C_{17})$ which increases ED (0.39e) that weakens the respective bonds leading to stabilization of 26.25 kcal mol^{-1}. Also another intra molecular hyper conjugative interactions are formed by the orbital overlap between n(N) and π*(N—C) bond orbital which results in ICT causing stabilization of the system. The strong intra molecular hyper conjugative interaction of N_{10}—C_{12} from of $n_1(N_{11}) \rightarrow \pi^*(N_{10}$—$C_{12})$ which increases ED (0.35e) that weakens the respective bonds leading to stabilization of 50.13 kcal mol^{-1}. These interactions are observed as an increase in electron density (ED) in C—C, N—C anti-bonding orbital that weakens the respective bonds.

The increased electron density at the oxygen atoms leads to the elongation of respective bond length and a lowering of the corresponding stretching wavenumber. The electron density (ED) is transferred from the n(O), n(N) to the anti-bonding π* orbital of the C—C, N—C explaining both the elongation and the red shift. The —CH_2O stretching modes can be used as a good probe for evaluating the bonding configuration around the corresponding atoms and the electronic distribution of the benzene molecule. Hence the 2-(phenoxymethyl)benzimidazole structure is stabilized by these orbital interactions. The NBO analysis also describes the bonding in terms of the natural hybrid orbital $n_2(O_{26})$, which occupy a higher energy orbital (−0.32017 a.u.) with considerable p-character (100.00%) and low occupation number (1.86649 a.u.) and the other $n_1(O_{26})$ occupy a lower energy orbital (−0.56367) with p-character (58.92%) and high occupation number (1.96434 a.u.). Also $n_1(N_{11})$, which occupy a higher energy orbital (−0.26494 a.u.) with considerable p-character (100.00%) and low occupation number (1.61117 a.u.) and the other $n_1(N_{10})$ occupy a lower energy orbital (−0.34026) with p-character (66.51%) and high occupation number (1.92659 a.u.). Thus, a very close to pure p-type lone pair orbital participates in the electron donation to the σ*(C—C) orbital for $n_2(O_{26}) \rightarrow \sigma^*$(C—C) and σ*(N—C) orbital for $n_1(N_{11}) \rightarrow \sigma^*$(N—C), $n_1(N_{10}) \rightarrow \sigma^*$(N—C) interactions in the compound. The results are tabulated in Table 3.

Mulliken charges and Molecular Electrostatic Potential

The calculation of atomic charges plays an important role in the application of quantum mechanical calculations to molecular systems. Mulliken charges are calculated by determining the electron population of each atom as defined in the basis functions. The charge distributions calculated by the Mulliken [90] and NBO methods for the equilibrium geometry of 2-(phenoxymethyl)benzimidazole are given in Table S2 (Supporting material). The charge distribution on the molecule has an important influence on the vibrational spectra. In 2-(phenoxymethyl)benzimidazole, the Mulliken atomic charge of the carbon atoms in the neighborhood of C_3, C_4, C_{12}, C_{16} become more positive, shows the direction of delocalization and shows that the natural atomic charges are more sensitive to the changes in the molecular structure than Mulliken's net charges. The results are represented in Fig. S3 (Supporting

Table 3
NBO results showing the formation of Lewis and non-Lewis orbitals.

Bond(A—B)	ED/energy	EDA%	EDB%	NBO	s%	p%
σC1—C2	1.97573	49.34	50.66	$0.7024(sp^{1.84})C$	35.20	64.80
–	−0.68572	–	–	$+0.7118\ (sp^{1.82})C$	35.75	64.25
πC1—C2	1.72789	48.98	51.02	$0.6999(sp^{1.00})C$	0.00	100.0
–	−0.24455	–	–	$+0.7143(sp^{1.00})C$	0.00	100.0
σC1—C6	1.98049	50.14	49.86	$0.7081(sp^{1.84})C$	35.19	64.81
–	−0.67402	–	–	$+0.7061(sp^{1.87})C$	34.84	65.16
σC2—C3	1.97583	48.46	51.54	$0.6961(sp^{1.96})C$	33.80	66.20
–	−0.70631	–	–	$+0.7179(sp^{1.50})C$	39.96	60.04
σC3—C4	1.96899	51.03	48.97	$0.7143(sp^{2.04})C$	32.93	67.07
–	−0.67221	–	–	$+0.6998(sp^{2.08})C$	32.45	67.55
πC3—C4	1.60257	49.88	50.12	$0.7062(sp^{1.00})C$	0.00	100.0
–	−0.24485	–	–	$+0.7080(sp^{1.00})C$	0.00	100.0
σC3—N11	1.98380	38.42	61.58	$0.6199(sp^{2.71})C$	26.95	73.05
–	−0.79917	–	–	$+0.7847(sp^{1.87})N$	34.88	65.12
σC4—C5	1.96660	51.13	48.87	$0.7150(sp^{1.59})C$	38.64	61.36
–	−0.69048	–	–	$+0.6991(sp^{1.93})C$	34.13	65.87
σC4—N10	1.97651	42.07	57.93	$0.6486(sp^{2.49})C$	28.67	71.33
–	−0.74842	–	–	$+0.7611(sp^{2.21})N$	31.11	68.89
σC5—C6	1.97755	50.28	49.72	$0.7091(sp^{1.82})C$	35.47	64.53
–	−0.68230	–	–	$+0.7051(sp^{1.82})C$	35.43	64.57
πC5—C6	1.71464	48.75	51.25	$0.6982(sp^{1.00})C$	0.00	100.0
–	−0.23830	–	–	$+0.7159(sp^{1.00})C$	0.00	100.0
σN10—C12	1.98424	57.93	42.07	$0.7611(sp^{1.82})N$	35.41	64.59
–	−0.84684	–	–	$+0.6486(sp^{1.93})C$	34.07	65.93
πN10—C12	1.88015	58.61	41.39	$0.7656(sp^{1.00})N$	0.00	100.0
–	−0.30334	–	–	$+0.6433(sp^{1.00})C$	0.00	100.0
σN11—C12	1.98725	62.20	37.8	$0.7887(sp^{1.97})N$	33.68	66.32
–	−0.81353	–	–	$+0.6148(sp^{2.37})C$	29.66	70.34
σC12—C13	1.97985	50.06	49.94	$0.7076(sp^{1.76})C$	36.25	63.75
–	−0.68000	–	–	$+0.7066(sp^{2.43})C$	29.15	70.85
σC13—O26	1.98962	32.19	67.81	$0.5673(sp^{4.28})C$	18.95	81.05
–	−0.80877	–	–	$+0.8235(sp^{2.75})O$	26.68	73.32
σC16—C17	1.97971	50.26	49.74	$0.7090(sp^{1.59})C$	38.62	61.38
–	−0.72021	–	–	$+0.7053(sp^{1.94})C$	33.97	66.03
πC16—C17	1.67651	47.53	52.47	$0.6894(sp^{1.00})C$	0.00	100.0
–	−0.26698	–	–	$+0.7244(sp^{1.00})C$	0.00	100.0
σC16—C18	1.97428	50.67	49.33	$0.7118(sp^{1.66})C$	37.55	62.45
–	−0.70950	–	–	$+0.7024(sp^{1.95})C$	33.92	66.08
σC16—O26	1.99132	32.16	67.84	$0.5671(sp^{3.23})C$	23.66	76.34
–	−0.88792	–	–	$+0.8237(sp^{2.10})O$	32.23	67.77
σC17—C19	1.97455	50.64	49.36	$0.7116(sp^{1.79})C$	35.80	64.20
–	−0.69612	–	–	$+0.7026(sp^{1.88})C$	34.75	65.25
σC18—C21	1.97626	50.34	49.66	$0.7095(sp^{1.779})C$	35.87	64.13
–	−0.69965	–	–	$+0.7047(sp^{1.86})C$	35.02	64.98
πC18—C21	1.69757	51.69	48.31	$0.7190(sp^{1.00})C$	0.00	100.0
–	−0.25426	–	–	$+0.6951(sp^{1.00})C$	0.00	100.0
σC19—C23	1.98067	50.20	49.80	$0.7085(sp^{1.81})C$	35.54	64.46
–	−0.69617	–	–	$+0.7057(sp^{1.86})C$	35.01	64.99
πC19—C23	1.68202	48.61	51.39	$0.6972(sp^{1.00})C$	0.00	100.0
–	−0.25090	–	–	$+0.7169(sp^{1.00})C$	0.00	100.0
σC21—C23	1.98036	50.17	49.83	$0.7083(sp^{1.84})C$	35.22	64.78
–	−0.69173	–	–	$+0.7059(sp^{1.88})C$	34.77	65.23
n1N10	1.92659	–	–	$sp^{1.99}$	33.49	66.51
–	−0.34026	–	–	–	–	–
n1N11	1.61117	–	–	$sp^{1.00}$	0.00	100.0
–	−0.26494	–	–	–	–	–
n1O26	1.96434	–	–	$sp^{1.43}$	41.08	58.92
–	−0.56367	–	–	–	–	–
n2O26	1.86649	–	–	$sp^{1.00}$	0.00	100.0
–	−0.32017	–	–	–	–	–

material). Also we done a comparison of Mulliken charges obtained by different basic sets and tabulated it in Table S3 (Supporting material) in order to assess the sensitivity of the calculated charges to changes in (i) the choice of the basis set; (ii) the choice of the quantum mechanical method. The results can, however, better be represented in graphical form as shown in Fig. S4 (Supporting material). We have observed a change in the charge distribution by changing different basis sets.

MEP is related to the ED and is a very useful descriptor in understanding sites for electrophilic and nucleophilic reactions as well as hydrogen bonding interactions [91,92]. The electrostatic potential $V(r)$ is also well suited for analyzing processes based on the "recognition" of one molecule by another, as in drug-receptor, and enzyme-substrate interactions, because it is through their potentials that the two species first "see" each other [93,94]. To predict reactive sites of electrophilic and nucleophilic attacks for the investigated molecule, MEP at the B3LYP/6-31G(d,p) optimized geometry was calculated. The negative (red and yellow[1]) regions of MEP were related to electrophilic reactivity and the positive (blue) regions to nucleophilic reactivity (Fig. 4). From the MEP it is evident

[1] For interpretation of color in Fig. 4, the reader is referred to the web version of this article.

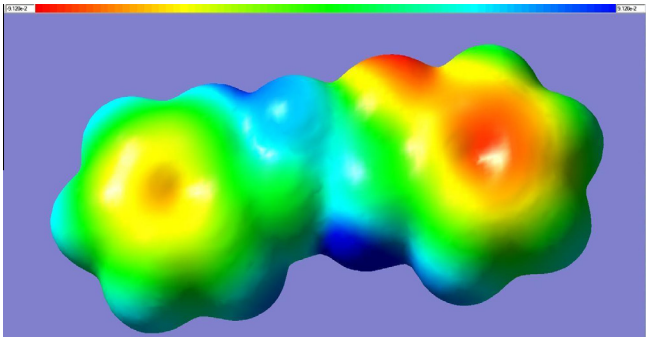

Fig. 4. Molecular Electrostatic Potential calculated at B3LYP/SDD level.

Table 4
Experimental and calculated ^{1}H NMR parameters (with respect to TMS).

Proton	σ_{TMS}	$\sigma_{calc.}$	$\delta(\sigma_{TMS} - \sigma_{calc.})$	Exp. δ_{ppm}
H7	32.7711	25.0344	7.7367	7.661
H8	–	25.0101	7.761	7.602
H9	–	25.2600	7.5111	7.517
H14	–	27.3373	5.4338	5.316
H15	–	27.3370	5.4341	5.313
H20	–	25.8637	6.9074	6.955
H22	–	25.4320	7.3391	7.339
H24	–	25.1317	7.6394	7.552
H25	–	25.1421	7.629	7.550
H27	–	23.3079	9.4632	9.512
H28	–	25.4570	7.3141	7.317
H29	–	25.2517	7.5194	7.552

that the negative charge covers the —CH_2O— group and the positive region is over the methoxyl group. The more electro negativity methoxy makes it the most reactive part in the molecule.

^{1}H NMR spectrum

The experimental spectrum data of 2-(phenoxymethyl)benzimidazole in DMSO with TMS as internal standard is obtained at 400 MHz and is displayed in Table 4. The absolute isotropic chemical shielding of 2-(phenoxymethyl)benzimidazole was calculated by B3LYP/GIAO model [95]. Relative chemical shifts were then estimated by using the corresponding TMS shielding: $\sigma_{calc.}$(TMS) calculated in advance at the same theoretical level as this article. Numerical values of chemical shift $\delta_{calc.} = \sigma_{calc.}(TMS) - \sigma_{calc.}$ together with calculated values of $\sigma_{calc.}$(TMS), are reported in Table 4. It could be seen from Table 4 that chemical shift was in agreement with the experimental ^{1}H NMR data. Thus, the results showed that the predicted proton chemical shifts were in good agreement with the experimental data for 2-(phenoxymethyl) benzimidazole.

Electronic absorption spectra

Electronic transitions are usually classified according to the orbital engaged or to specific parts of the molecule involved. Common types of electronic transitions in organic compounds are π–π^*, n–π^* and π^*(acceptor)–π(donor). The UV–visible bands in 2-(phenoxymethyl)benzimidazole are observed at 280, 275, 271, 260, 235 and 228 nm. Observed band at 228 nm is due to the π–π^*. The less intense band centered at 271 nm is due to the partly forbidden n–π^* transition from HOMO to LUMO. The more intense band observed at 280 nm belonged to the dipole-allowed π–π^* transition. In order to understand the electronic transitions of 2-(phenoxymethyl)benzimidazole, TD-DFT calculation on electronic absorption spectrum in vacuum was performed. TD-DFT calculation is capable of describing the spectral features of 2-(phenoxymethyl)benzimidazole because of the qualitative agreement of line shape and relative strength as compared with experiment. The absorption spectra of organic compounds stem from the ground-to-excited state vibrational transition of electrons. The intense band in the UV range of the electronic absorption spectrum is observed at 280 nm, which is indicating the presence of —OPh entity in the compound. The calculated six lowest-energy transitions of the molecule from TD-DFT method and the observed electronic transitions are listed in Table 5. From the table the calculated energy transitions are red shifted from the experimental value, because these bands are observed in gas phase without considering the solvent effect.

HOMO and LUMO are the very important parameters for quantum chemistry. The conjugated molecules are characterized by a highest occupied molecular orbital–lowest unoccupied molecular orbital (HOMO–LUMO) separation, which is the result of a significant degree of ICT from the end-capping electron-donor groups to the efficient electron-acceptor groups through π-conjugated path. The strong charge transfer interaction through π-conjugated bridge results in substantial ground state donor–acceptor mixing and the appearance of a charge transfer band in the electronic absorption spectrum. Therefore, an ED transfer occurs from the

Table 5
Calculated electronic absorption spectrum of using TD-DFT/B3LYP/SDD.

Excitation	CI expansion	Energy coefficient (eV)	Wavelength (nm)		Oscillator strength (f)
			Calculated	Expt.	
Excited State 1					
58 → 60	0.52516	5.0052	247.71	280	0.1053
58 → 61	0.19018	–	–	–	–
58 → 63	0.11162	–	–	–	–
59 → 60	0.19449	–	–	–	–
59 → 63	−0.34041	–	–	–	–
Excited State 2					
56 → 62	0.16412	5.04521	245.75	275	0.0559
57 → 60	0.19818	–	–	–	–
57 → 61	−0.14689	–	–	–	–
58 → 60	−0.19048	–	–	–	–
58 → 63	0.13579	–	–	–	–
59 → 60	0.54882	–	–	–	–
59 → 61	−0.11583	–	–	–	–
Excited State 3					
56 → 62	0.28405	5.0824	243.95	271	0.0665
57 → 60	0.34847	–	–	–	–
57 → 61	−0.33750	–	–	–	–
58 → 61	0.17621	–	–	–	–
58 → 63	−0.10953	–	–	–	–
59 → 60	−0.25591	–	–	–	–
59 → 61	−0.15964	–	–	–	–
Excited State 4					
57 → 60	0.17195	5.1337	241.51	260	0.0054
58 → 60	−0.13442	–	–	–	–
58 → 61	0.10425	–	–	–	–
58 → 63	0.11023	–	–	–	–
59 → 61	0.62198	–	–	–	–
Excited State 5					
57 → 60	−0.38773	5.2076	238.08	235	0.0022
57 → 61	−0.13865	–	–	–	–
58 → 60	−0.19916	–	–	–	–
58 → 61	0.51220	–	–	–	–
Excited State 6					
56 → 62	−0.11042	5.2980	234.02	228	0.0261
57 → 60	0.31655	–	–	–	–
57 → 61	0.46781	–	–	–	–
58 → 60	−0.17185	–	–	–	–
58 → 61	0.29847	–	–	–	–
59 → 61	−0.11388	–	–	–	–

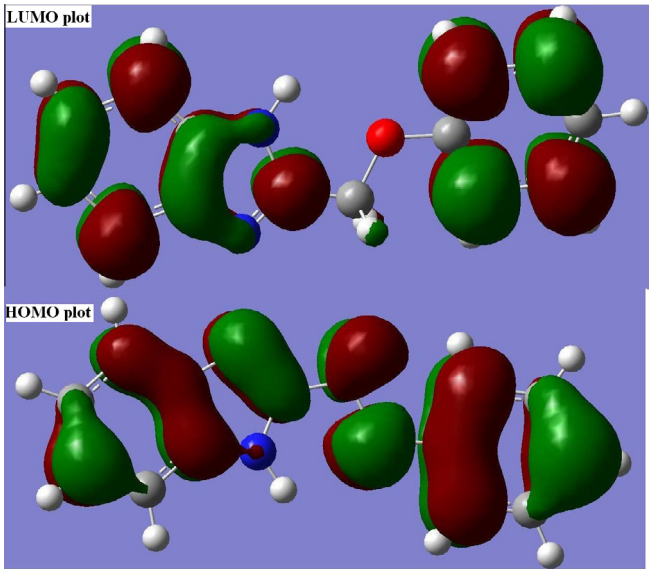

Fig. 5. HOMO, LUMO plots of 2-(phenoxymethyl)benzimidazole.

more aromatic part of the π-conjugated system in the electron-donor side to its electron-withdrawing part. The atomic orbital components of the frontier molecular orbital are shown in Fig. 5. The HOMO–LUMO energy gap value is found to be 3.916 eV, which is responsible for the bioactive property of the compound 2-(phenoxymethyl)benzimidazole [96].

Conclusion

The geometry optimizations have been carried out using HF and DFT levels and are in agreement with the reported values. The normal modes are assigned by PED calculations. The simultaneous activation of the phenyl ring stretching modes in IR and Raman spectra can be interpreted as the evidence of intra molecular charge transfer between the donor and the acceptor group via conjugated ring path, which is responsible for hyperpolarizability enhancement, leading to non-linear optical activity. The NBO analysis confirms the ICT formed by the orbital overlap between n(O) and π^*(C—C), n(N) and π^*(N—C). A very close to pure p-type lone pair orbital participates in the electron donation to the σ^*(C—C) orbital for $n_2(O_{26}) \rightarrow \sigma^*$(C—C) and σ^*(N—C) orbital for $n_1(N_{11}) \rightarrow \sigma^*$(N—C), $n_1(N_{10}) \rightarrow \sigma^*$(N—C) interaction in the molecule. Overall, the TD-DFT calculations on the molecule provided deep insight into their electronic structures and properties. GIAO-NMR calculations provided chemical shift values that were in excellent agreement with experimental data. In addition, the calculated UV–Vis results are all in good agreement with the experimental data. The lowering of HOMO–LUMO band gap supports bioactive property of the molecule. MEP predicts the most reactive part in the molecule.

Acknowledgments

S.A. and I.Y. would like to thank the Research Fund of Ankara University (Grant No. 12B3336002) for the financial support in this research. The authors are thankful to University of Antwerp for access to the university's CalcUA Supercomputer Cluster.

Appendix A. Supplementary material

Supplementary data associated with this article can be found, in the online version, at http://dx.doi.org/10.1016/j.saa.2014.01.068.

References

[1] R.L. Lombardy, F.A. Tanious, K. Ramachandran, R.R. Tidwell, W.D. Wilson, J. Med. Chem. 39 (1996) 1452–1462.
[2] M.J. Tebbe, W.A. Spitzer, F. Victor, S.C. Miller, C.C. Lee, T.R. Sattelberg, E. McKinney, J.C. Tang, J. Med. Chem. 40 (1997) 3937–3946.
[3] A.R. Porcari, R.V. Devivar, L.S. Kucera, J.C. Drach, L.B. Townsend, J. Med. Chem. 41 (1998) 1252–1262.
[4] T.C. Kuhler, M. Swanson, V. Shcherbuchin, H. Larsson, B. Mellgard, J.E. Sjostrom, J. Med. Chem. 41 (1998) 1777–1788.
[5] I. Tapia, L. Alonso-Cires, P.L. Lopez-Tudanca, R. Mosquera, L. Labeaga, A. Innerarity, A. Orjales, J. Med. Chem. 42 (1999) 2870–2880.
[6] J.J. Chen, Y. Wie, J.C. Drach, L.C. Townsend, J. Med. Chem. 43 (2000) 2449–2456.
[7] A.W. White, R. Almassy, A.H. Calvert, N.J. Curtin, R.J. Griffin, Z. Hostomsky, K. Maegley, D.R. Newell, S. Srinivasan, B.T. Golding, J. Med. Chem. 43 (2000) 4084–4097.
[8] W. Roth, D. Spangenberg, C. Janzen, A. Westphal, M. Schmitt, Chem. Phys. 248 (1999) 17–25.
[9] E. Jalviste, A. Treshchalov, Chem. Phys. 172 (1993) 325–338.
[10] B.C. Bishop, E.T.J. Chelton, A.S. Jones, Biochem. Pharmacol. 13 (1964) 751–754.
[11] N.S. Habib, R. Soliman, F.A. Ashoura, M. El-Taiebi, Pharmazie 52 (1997) 746–749.
[12] I. Oren, O. Temiz, I. Yalcin, E. Sener, A. Akin, N. Altanlar, Eur. J. Pharm. Sci. 7 (1998) 153–160.
[13] H. Goker, M. Tuncbilek, S. Suzen, C. Kus, N. Altanlar, Arch. Pharm. Pharm. Med. Chem. 334 (2001) 148–152.
[14] H. Goker, C. Kus, D.W. Boykin, S. Yildiz, N. Altanlar, Bioorg. Med. Chem. 10 (2002) 2589–2596.
[15] N.S. Pawar, D.S. Dalal, S.R. Shimpi, P.P. Mahulikar, Eur. J. Pharm. Sci. 21 (2004) 115–118.
[16] B.G. Mohammad, M.A. Hussein, A.A. Abdel-Alim, M. Hashem, Arch. Pharm. Res. 29 (2006) 26–33.
[17] S.D. Vaidya, B.V.S. Kumar, R.V. Kumar, U.N. Bhise, U.C. Mashelkar, J. Heterocycl. Chem. 44 (2007) 685–691.
[18] P.N. Preston, Chem. Rev. 74 (1974) 279–314.
[19] R. Dubey, S. Abuzar, S. Sharma, R.K. Chatterjee, J.C. Katiyar, J. Med. Chem. 28 (1985) 1748–1750.
[20] E.S. Lazer, M.R. Matteo, G.J. Possanza, J. Med. Chem. 30 (1987) 726–729.
[21] H. Nakano, T. Inoue, N. Kawasaki, H. Miyataka, H. Matsumoto, T. Taguchi, N. Inagaki, H. Nagai, T. Satoh, Chem. Pharm. Bull. 47 (1999) 1573–1578.
[22] A.H. El-Masry, H.H. Fahmy, S.H.A. Abdelwahed, Molecules 5 (2000) 1429–1438.
[23] M. Castelli, M. Malagoli, L. Lupo, T.R. Riccomi, C. Casolari, C. Cermelli, A. Zanca, G. Baggio, Pharm. Toxicol. 88 (2001) 67–74.
[24] D.G. Joshi, H.B. Oza, H.H. Parekh, Ind. J. Heterocycl. Chem. 11 (2001) 145–148.
[25] Z. Kazimierczuk, J.A. Upcroft, P. Upcroft, A. Gorska, B. Starosciak, A. Laudy, Acta Biochim. Polon. 49 (2002) 185–195.
[26] N.M. Goudgaon, V. Dhondiba, A. Vijayalaxmi, Ind. J. Heterocycl. Chem. 13 (2004) 271–272.
[27] H. Goker, S. Ozden, S. Yildiz, D.W. Boykin, Eur. J. Med. Chem. 40 (2005) 1062–1069.
[28] R.V. Kumar, K.R. Gopal, K.V.S.R.S. Kumar, J. Heterocycl. Chem. 42 (2005) 1405–1408.
[29] K. Starcevic, M. Kralj, K. Ester, I. Sabol, M. Grce, K. Pavelic, G. Karminski-Zamola, Bioorg. Med. Chem. 15 (2007) 4419–4426.
[30] H. Wenmian, F. Jian, Z. Zhengzhi, Biol. Trace Element Res. 64 (1998) 27–35.
[31] J. Cheng, J. Xie, X. Luo, Bioorg. Med. Chem. Lett. 15 (2005) 267–269.
[32] Y. He, J. Yang, B. Wu, L. Risen, E.E. Swayze, Bioorg. Med. Chem. Lett. 14 (2004) 1217–1220.
[33] M.A. Ismail, R. Brun, T. Wenzler, F.A. Tanious, W.D. Wilson, D.W. Boykin, Bioorg. Med. Chem. 12 (2004) 5405–5413.
[34] H. Nakano, T. Inoue, N. Kawasaki, H. Miyataka, H. Matsumoto, T. Taguchi, N. Inagaki, H. Nagai, T. Satoh, Bioorg. Med. Chem. 8 (2000) 373–380.
[35] R. Marquis, J. Sheng, T. Nguyen, J. Baldeck, J. Olsson, Arch. Oral Biol. 51 (2006) 1015–1023.
[36] A.T. Mavrova, K.K. Anichina, D.I. Vuchev, J.A. Tsenov, P.S. Denkova, M.S. Kondeva, M.K. Micheva, Eur. J. Med. Chem. 41 (2006) 1412–1420.
[37] S.O. P odunavac-Kuzmonovic, V.M. Leovac, N.U. Perisic-Janjic, J. Rogan, J. Balaz, J. Serb, Chem. Soc. 64 (1999) 381–384.
[38] M. Boiani, M. Gonzalez, Mini Rev. Med. Chem. 5 (2005) 409–424.
[39] I. Yildiz-Oren, I. Yalcin, E. Aki-Sener, N. Ucarturk, Eur. J. Med. Chem. 39 (2004) 291–298.
[40] F.E. King, R.M. Acheson, J. Chem. Soc. (1949) 1396–1400.
[41] I. Yalcin, E. Sener, T. Ozden, S. Ozden, A. Akin, Eur. J. Med. Chem. 25 (1990) 705–708.
[42] M.A. Phillips, J. Chem. Soc. (1928) 2393–2399.
[43] Gaussian 09, Revision B.01, M.J. Frisch, G.W. Trucks, H.B. Schlegel, G.E. Scuseria, M.A. Robb, J.R. Cheeseman, G. Scalmani, V. Barone, B. Mennucci, G.A. Petersson, H. Nakatsuji, M. Caricato, X. Li, H.P. Hratchian, A.F. Izmaylov, J. Bloino, G. Zheng, J.L. Sonnenberg, M. Hada, M. Ehara, K. Toyota, R. Fukuda, J. Hasegawa, M. Ishida, T. Nakajima, Y. Honda, O. Kitao, H. Nakai, T. Vreven, J.A. Montgomery Jr., J.E. Peralta, F. Ogliaro, M. Bearpark, J.J. Heyd, E. Brothers, K.N. Kudin, V.N. Staroverov, T. Keith, R. Kobayashi, J. Normand, K. Raghavachari, A. Rendell, J.C. Burant, S.S. Iyengar, J. Tomasi, M. Cossi, N. Rega, J.M. Millam, M. Klene, J.E. Knox, J.B. Cross, V. Bakken, C. Adamo, J. Jaramillo, R. Gomperts, R.E.

Stratmann, O. Yazyev, A.J. Austin, R. Cammi, C. Pomelli, J.W. Ochterski, R.L. Martin, K. Morokuma, V.G. Zakrzewski, G.A. Voth, P. Salvador, J.J. Dannenberg, S. Dapprich, A.D. Daniels, O. Farkas, J.B. Foresman, J.V. Ortiz, J. Cioslowski, D.J. Fox, Gaussian Inc., Wallingford, CT, 2010.
[44] J.B. Foresman, in: E. Frisch (Ed.), Exploring Chemistry with Electronic Structure Methods: A Guide to Using Gaussian, Gaussian Inc., Pittsburg, PA, 1996.
[45] P.J. Hay, W.R. Wadt, J. Chem. Phys. 82 (1985) 270–283.
[46] J.Y. Zhao, Y. Zhang, L.G. Zhu, J. Mol. Struct. Theochem. 671 (2004) 179–187.
[47] GaussView, Version 5, R. Dennington, T. Keith, J. Millam, Semichem Inc., Shawnee Mission KS, 2009.
[48] J.M.L. Martin, C. Van Alsenoy, GAR2PED, A Program to Obtain a Potential Energy Distribution from a Gaussian Archive Record, University of Antwerp, Belgium, 2007.
[49] P.L. Anto, C.Y. Panicker, H.T. Varghese, D. Philip, O. Temiz-Arpaci, B. Tekiner-Gulbas, I. Yildiz, Spectrochim. Acta 67 (2007) 744–749.
[50] R. Saxena, L.D. Kandpal, G.N. Mathur, J. Polym. Sci. A: Polym. Chem. 40 (2002) 3959–3966.
[51] R.M. Silverstein, G.C. Bassler, T.C. Morril, Spectrometric Identification of Organic Compounds, fifth ed., John Wiley and Sons Inc., Singapore, 1991.
[52] K. Nakamoto, Infrared and Raman spectrum of Inorganic and Coordination Compounds, fifth ed., John Wiley and Sons Inc., New York, 1997.
[53] T.D. Klots, W.B. Collier, Spectrochim. Acta 51A (1995) 1291–1316.
[54] G. Yang, S. Matsuzono, E. Koyama, H. Tokuhisa, K. Hiratani, Macromolecules 34 (2001) 6545–6547.
[55] J.B. Bhagyasree, H.T. Varghese, C.Y. Panicker, J. Samuel, C. Van Alsenoy, K. Bolelli, I. Yildiz, E. Aki, Spectrochim. Acta 102 (2013) 99–113.
[56] N.P.G. Roeges, A Guide to the Complete Interpretation of Infrared Spectra of Organic Structures, John Wiley and Sons Inc., New York, 1994.
[57] G. Socrates, Infrared Characteristic Group Frequencies, John Wiley and Sons, New York, 1981.
[58] A. Spire, M. Barthes, H. Kallouai, G. De Nunzio, Physics D 137 (2000) 392–396.
[59] R. Minitha, Y.S. Mary, H.T. Varghese, C.Y. Panicker, R. Ravindran, K. Raju, V.M. Nair, J. Mol. Struct. 985 (2011) 316–322.
[60] C.Y. Panicker, H.T. Varghese, V.S. Madhavan, S. Mathew, J. Vinsova, C. Van Alsenoy, Y.S. Mary, Y.S. Mary, J. Raman Spectrosc. 40 (2009) 2176–2186.
[61] M.S. Kim, M.K. Kim, C.J. Lee, Y.M. Jung, M.S. Lee, Bull. Korean Chem. Soc. 30 (2009) 2930–2934.
[62] K. Malek, A. Puc, G. Schroeder, V.I. Rybachenko, L.M. Proniewich, Chem. Phys. 327 (2006) 439–451.
[63] N.B. Colthup, L.H. Daly, S.E. Wiberly, Introduction to Infrared and Raman Spectroscopy, second ed., Academic Press, New York, 1975.
[64] N. Sandhyarani, G. Skanth, S. Berchmanns, V. Yegnaraman, T. Pradeep, J. Colloid Interface Sci. 209 (1999) 154–161.
[65] A. Bigotto, B. Pergolese, J. Raman Spectrosc. 32 (2001) 953–959.
[66] J. Coates, in: R.A. Meyers (Ed.), Interpretation of Infrared Spectra, A Practical Approach, John Wiley and Sons Inc., Chichester, 2000.
[67] A. Raj, Y.S. Mary, C.Y. Panicker, H.T. Varghese, K. Raju, Spectrochim. Acta 113 (2013) 23–36.
[68] M. Kaur, Y.S. Mary, H.T. Varghese, C.Y. Panicker, H.S. Yathirajan, M.S. Siddegowda, C. Van Alsenoy, Spectrochim. Acta 98 (2012) 91–99.
[69] V.S. Madhavan, Y.S. Mary, H.T. Varghese, C.Y. Panicker, S. Mathew, C. Van Alsenoy, J. Vinsova, Spectrochim. Acta 89 (2012) 308–316.
[70] T. Joseph, H.T. Varghese, C.Y. Panicker, T. Thiemann, K. Viswanathan, C. Van Alsenoy, J. Mol. Struct. 1005 (2011) 17–24.
[71] Y.S. Mary, C.Y. Panicker, H.T. Varghese, K. Raju, T.E. Bolelli, I. Yildiz, C.M. Granadeiro, H.I.S. Nogueira, J. Mol. Struct. 994 (2011) 223–231.
[72] H.T. Varghese, C.Y. Panicker, V.S. Madhavan, S. Mathew, J. Vinsova, C. Van Alsenoy, J. Raman Spectrosc. 40 (2009) 1211–1223.
[73] G. Varsanyi, Assignments of Vibrational Spectra of Seven Hundred Benzene Derivatives, John Wiley and Sons Inc., New York, 1974.
[74] C.Y. Panicker, H.T. Varghese, K.R. Ambujakshan, S. Mathew, S. Ganguli, A.K. Nanda, C. Van Alsenoy, Y.S. Mary, J. Mol. Struct. 963 (2010) 137–144.
[75] S. Higuchi, H. Tsuyama, S. Tanaka, H. Kamada, Spectrochim. Acta 30 (1974) 463–477.
[76] J. Chowdhury, J. Sarkar, R. De, M. Ghosh, G.B. Talapatra, Chem. Phys. 330 (2006) 172–183.
[77] J. Sarkar, J. Chowdhury, M. Ghosh, R. De, G.B. Talapatra, J. Phys. Chem. 109B (2005) 22536–22544.
[78] P. Purkayastha, N. Chattopadhyay, Phys. Chem. Chem. Phys. 2 (2000) 203–210.
[79] P. Sykes, A Guide Book to Mechanism in Organic Chemistry, sixth ed., Pearson Education, India, 2004.
[80] H. Arslan, U. Florke, N. Kulcu, G. Binzet, Spectrochim. Acta 68A (2007) 1347–1355.
[81] A. Lifshitz, C. Tamburu, A. Suslensky, F. Dubnikova, J. Phys. Chem. A 110 (2006) 4607–4613.
[82] K.R. Ambujakshan, V.S. Madhavan, H.T. Varghese, C.Y. Panicker, O. Temiz-Arpaci, B. Tekiner-Gulbas, I. Yildiz, Spectrochim. Acta, Part A: Mol. Biomol. Spectrosc. 69 (2008) 782–788.
[83] Y.R. Shen, The Principles of Nonlinear Optics, Wiley, New York, 1984.
[84] P.V. Kolinsky, Opt. Eng. 31 (1992) 1676–1684.
[85] D.F. Eaton, Science 253 (1991) 281–287.
[86] D.A. Kleinman, Phys. Rev. 126 (1962) 1977–1979.
[87] L.N. Kuleshova, M.Y. Antipin, V.N. Khrustalev, D.V. Gusev, G.V. Grintselev-Knyazev, E.S. Bobrikova, Cryst. Rep. 48 (2003) 594–601.
[88] C. Adant, M. Dupuis, J.L. Bredas, Int. J. Quantum Chem. 56 (1995) 497–507.
[89] NBO Version 3.1, E.D. Glendening, A.E. Reed, J.E .Carpenter, F. Weinhold.
[90] R.S. Mulliken, J. Chem. Phys. 23 (1955) 1833–1840.
[91] E. Scrocco, J. Tomasi, Adv. Quantum Chem. 11 (1978) 115–193.
[92] F.J. Luque, J.M. Lopez, M. Orozco, *Theor. Chem. Acc.* 103 (2000) 343–345.
[93] P. Politzer, J.S. Murray, in: D.L. Beveridge, R. Lavery (Eds.), Theoretical Biochemistry and Molecular Biophysics: A Comprehensive Survey, vol. 2, Protein, Adenine Press, Schenectady, NY, 1991 (Chapter 13).
[94] E. Scrocco, J. Tomasi, Top. Curr. Chem. 42 (1973) 95–170.
[95] K. Wolinski, J.F. Hinton, P. Pulay, J. Am. Chem. Soc. 112 (1990) 8251–8260.
[96] A. Lakshmi, V. Balachandran, J. Mol. Struct. 1033 (2013) 40–50.